Some Calculations Concerning the Pseudo-Kikuchi Pattern Contrast from Tilted Crystals

P. Pirouz *

Department of Metallurgy, Imperial College, London SW7 2BP

(Z. Naturforsch. **29 a**, 1188–1197 [1974]; received May 5, 1974)

The theory of Hirsch und Humphreys [1] has been applied to calculate the contrast across pseudo-Kikuchi bands for tilted crystals. The crystallographic planes giving rise to the pattern are assumed to lie parallel to the undeflected electron beam. An asymmetry in contrast across individual bands is found, in agreement with experimental observations.

Intensity profiles and simulated patterns for several angles of tilt in the case of the undeflected beam perpendicular to the (111) reciprocal latice plane of a silicon crystal are presented.

1. Introduction

The quantitative description of pseudo-Kikuchi patterns has been considered by a number of authors (Vicario et al. [2]; Hirsch and Humphreys [1]; Reimer et al. [3]; Clarke and Howie [4]). All the treatments start by describing the behaviour of incident electrons in the crystal as a linear superposition of Bloch waves (§ 2). Subsequently the backscattering of electrons by means of inelastic processes is considered and an expression for the intensity of electrons scattered back out of the crystal is obtained. Most applications of these theories has been for the case of a crystal whose surface is normal to the crystallographic planes and the electrons are incident at near normal angles. In this case, all the theories result in intensity profiles which are symmetrical about the centre for the two edges of a band as would be expected experimentally. However it has been observed that when the crystal is tilted, an asymmetry in the contrast of opposite edges of a band arises. The edge on the "uphill" side becomes brighter, while the edge on the "downhill" side becomes darker as compared to the background (Booker [5]).

Some preliminary calculations by Spencer and Humphreys [6] indicated that this asymmetry may be explained by the theory of Hirsch and Humphreys [1]. In this paper, some independent calculations also based on this theory are presented. The equations are modified to take into account the specimen inclination and the results of calculations for various angles of tilt are given. Some simulated patterns constructed by grey-level techniques are also presented. The computations produce the asymmetry across the bands in agreement with experimental observations. An explanation of this asymmetry in terms of the effects of tilt on electron wavefields in the crystal is offered.

* Presently at Laboratoire Thermodynamique et Physico-Chimie Métallurgique – LA nº 29, Domaine Universitaire, BP. 44, *38401 St-Martin d'Heres*, France. Reprint requests to this address.

2. Diffraction of Fast Electrons in the Crystal

The basic equations of dynamical theory are obtained by the solution of time-independent Schrodinger equation in a periodic field (Hirsch et al. [7]),

$$\nabla^2 \psi(\boldsymbol{r}) = (8\pi^2 m e/h^2)\,[E + V(\boldsymbol{r})]\,\psi(\boldsymbol{r}) = 0\,. \quad (1)$$

e and m are the charge and mass of the electrons respectively. E is the total energy of the electron and $\boldsymbol{r}$ is a position vector in the crystal. The periodic crystal potential is expanded as a Fourier series as follws,

$$V(\boldsymbol{r}) = \sum_g V_g \exp\{2\pi i\, \boldsymbol{g}\cdot\boldsymbol{r}\} = \frac{h^2}{2 m e} \sum_g U_g \exp\{2\pi i\, \boldsymbol{g}\cdot\boldsymbol{r}\} \quad (2)$$

where V_g 's are the Fourier coefficients of potential and the summation extends over all the reciprocal lattice vectors $\overline{\boldsymbol{g}}$ in the crystal.

The solutions of Schrodinger equation in the periodic field are now written in the form of Bloch waves, $b^{(j)}(\boldsymbol{k}^{(j)}, \boldsymbol{r})$ where,

$$b^{(j)}(\overline{k}^{(j)}, \overline{r}) = \sum_g C_g{}^{(j)} \exp\{2\pi i(\boldsymbol{k}^{(j)} + \boldsymbol{g})\cdot\boldsymbol{r}\}\,. \quad (3)$$

Thus each Bloch wave is a combination of a number of plane waves of wave vectors $\boldsymbol{k}_g (= \boldsymbol{k} + \boldsymbol{g})$ and amplitudes C_g.

The total wave function of the incident electron in the crystal is then written as a superposition of

solutions such as (3),

$$\psi'(\boldsymbol{r}) = \sum_j \psi'^{(j)}\, b^{(j)}(\boldsymbol{k}^{(j)}, \boldsymbol{r}) \qquad (4)$$

where $\psi'^{(j)}$ denotes the excitation of the jth Bloch wave in the crystal. Substitution of (3) in the Schrodinger Eq. (1) gives the basic dynamical equations from which one may obtain the amplitude coefficients $C_g^{(j)}$ and the wave vectors $k_g^{(j)}$,

$$(K^2 - k_g^2) C_g + \sum{}' U_h C_{g-h} = 0 \qquad (5)$$

where

$$K^2 = (2\,m\,e\,E/h^2) + U_0\,. \qquad (6)$$

K is the mean wave vector of the incident electrons in the crystal after correction for the refraction by the mean crystal potential U_0.

The effects of inelastic scatterings[8] are taken into account by making the potential in the Schrodinger equation a complex quantity. The imaginary part of the complex potential $V'(\boldsymbol{r})$ is assumed to have the same dependence on position as $V(\boldsymbol{r})$ and may be also expanded as a Fourier series,

$$V'(\boldsymbol{r}) = \sum_g V_g' \exp\{2\pi i\, \boldsymbol{g}\cdot\boldsymbol{r}\}\,. \qquad (7)$$

The introduction of an imaginary potential into the Schrodinger equation results in a change $e\,\Delta E$ in the energy of the jth Bloch wave which may be found by the application of first order perturbation theory (Hirsch et al.[7]),

$$e\,\Delta E = -i\langle b^{(j)*}(\boldsymbol{k}, \boldsymbol{r}) \,|\, V'(\boldsymbol{r}) \,|\, b^{(j)}(\boldsymbol{k}, \boldsymbol{r}) \rangle\,. \qquad (8)$$

The wave vectors now acquire an imaginary component $i\,q$ in a direction normal to the crystal surface, i. e. $\boldsymbol{k}_g^{(j)} \rightarrow \boldsymbol{k}_g^{(j)} + i\,\boldsymbol{q}^{(j)}$ where,

$$i\,q^{(j)} = (m\,e/h^2\,k_\perp^{(j)})\,\Delta E\,. \qquad (9)$$

3. Calculation of Wave Vectors and Wave Amplitudes

In order to solve (5) for obtaining the values of $k_g^{(j)}$ and $C_g^{(j)}$ we shall first consider the geometry of the situation. In Fig. 1, it is assumed that the crystal is tilted through an angle α about the y-axis where the system of coordinates is fixed such that the z-axis is parallel to the undeflected direction of the beam and passing through $0''$. However, we can represent the observation screen by a hypothetical plane perpendicular to the undeflected direction and at a fictitious distance d from the crossover point A (see Figure 1). The distance d is directly proportional to the magnification of the microscope and the sides of the hypothetical plane are of length L which is also the size of the observation screen. At any instant during the scan, the orientation β of the incident beam relative to the undeflected direction is given by,

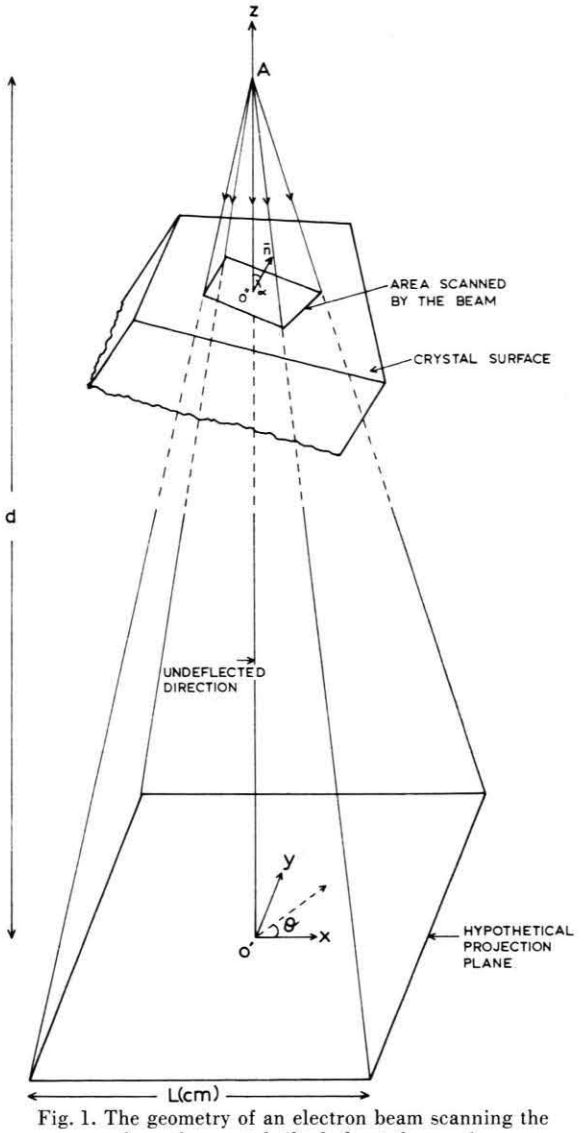

Fig. 1. The geometry of an electron beam scanning the surface of a crystal tilted about the y-axis.

$$\cos\beta = d/\sqrt{x^2 + y^2 + d^2} \qquad (10)$$

where x and y are coordinates of a point on the observation screen as defined in Fig. 1 and,

$$x \leqq \pm L\,; \qquad y \leqq \pm L\,.$$

In the case of zero tilt, of course, the surface of the crystal and the hypothetical plane are parallel.

We assume that only the reciprocal lattice points lying on the zero-order Laue zone are excited. Also, as mentioned in the introduction, it is assumed that this zone is normal to the incident beam, i. e. it is parallel to the hypothetical plane of Figure 1. This situation is shown in Fig. 2 which also shows two branches of the dispersion surface. The axes x', y' and z' are respectively parallel to the x, y and z axes of Figure 1. In this figure, $\boldsymbol{g}$ is a reciprocal lattice vector lying at an angle ω_g from the x' axis.

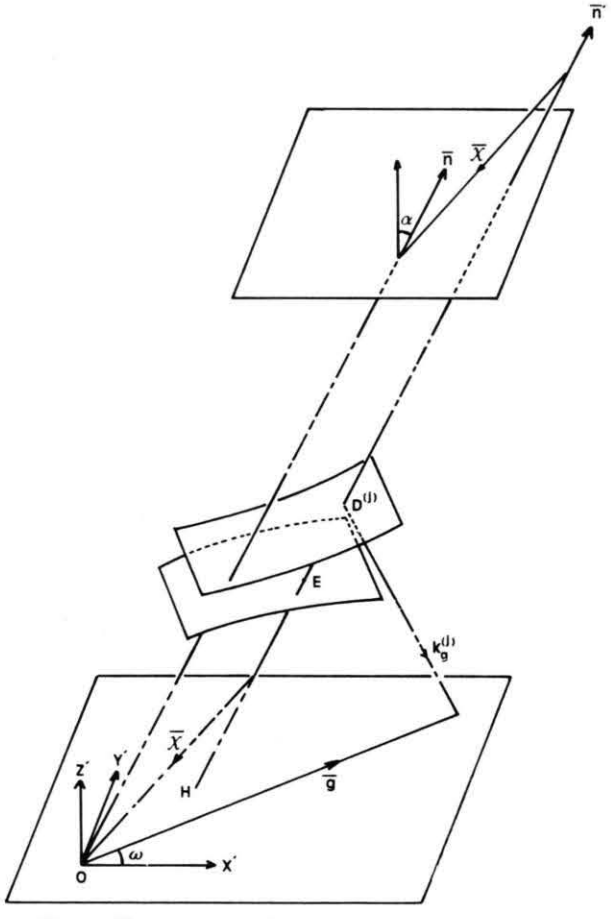

Fig. 2. The geometry of the situation in reciprocal space. Only two branches of the dispersion surface are drawn for clarity.

As the electron beam scans the surface of the crystal, the wave vectors of the Bloch waves excited in the crystal move on the various branches of the dispersion surface. In Fig. 2, the vacuum wave vector $\boldsymbol{\chi}$ at a particular instant during the scan is shown together with the normal to the crystal surface $\boldsymbol{n}$. H is the intersection of the vector $\boldsymbol{n}'$, parallel to $\boldsymbol{n}$, with the zero-order Laue zone. The vector $\boldsymbol{n}'$ corresponds to the instant during which the incident wave vector is represented by $\boldsymbol{\chi}$. The wave points of the Bloch waves are determined by the intersection of $\boldsymbol{n}'$ with the various branches of the dispersion surface. One such wave point on the jth branch is shown by D^j in Figure 2.

The equation of the normal $\boldsymbol{n}'$ can now be written as follows,

$$z' = (x' - x_{\mathrm{H}}') \cot \alpha \tag{11}$$

remembring that there is only a tilt α about the y'-axis. x_{H}', y_{H}', and z_{H}' are the coordinates of H and may be easily shown to be,

$$\begin{aligned} x_{\mathrm{H}}' &= \chi(\sin\beta\cos\sigma - \cos\beta\tan\alpha)\,, \\ y_{\mathrm{H}}' &= \chi\sin\beta\sin\sigma\,, \\ z_{\mathrm{H}}' &= 0\,. \end{aligned} \tag{12}$$

where,

$$\tan\sigma = y/x\,. \tag{13}$$

During the beam scan, the wave vector $\boldsymbol{K}$ moves on a section of a sphere whose intersection with $\boldsymbol{n}'$ is shown by E in Figure 2. The coordinates of E may be obtained by solving the equation of the sphere,

$$x'^2 + y'^2 + z'^2 = K^2 \tag{14}$$

with Equation (6). We thus obtain,

$$\begin{aligned} K_{x'} &= x_{\mathrm{H}}'\cos^2\alpha \pm \sin\alpha\sqrt{K^2 - y_{\mathrm{H}}'^2 - x_{\mathrm{H}}'^2\cos^2\alpha}\,, \\ K_{y'} &= y_{\mathrm{H}}'\,, \\ K_{z'} &= -\tfrac{1}{2}x_{\mathrm{H}}'\sin 2\alpha \pm \cos\alpha\sqrt{K^2 - y_{\mathrm{H}}'^2 - x_{\mathrm{H}}'^2\cos^2\alpha}\,. \end{aligned} \tag{15}$$

We now define the vector $\boldsymbol{\gamma}^{(j)}$ lying on the surface normal and where,

$$\boldsymbol{\gamma}^{(j)} = \boldsymbol{E}\,\boldsymbol{D}^{(j)}\,.$$

We then have that,

$$\boldsymbol{k}_g^{(j)} = \boldsymbol{K} + \boldsymbol{g} - \boldsymbol{\gamma}^{(j)}\,. \tag{16}$$

Squaring both sides and neglecting the term γ^2 which is very small except for angles greater than about 75°, we obtain,

$$K^2 - k_g^2 = S_g - \gamma^{(j)}\,T_g \tag{17}$$

where,

$$S_g = -g^2 + 2\,g(K_x\cos\omega_g + K_y\sin\omega_g) \tag{18 a}$$

$$T_g = 2[(K_x - g_x)\sin\alpha + K_z\cos\alpha]\,. \tag{18 b}$$

Substituting (17) in (5), we obtain,

$$(S_g/T_g)\,C_g^{(j)} + \sum{}' U_h\,C_{g-h}^{(j)} = \gamma^{(j)}\,C_g^{(j)} \tag{19}$$

which may be written in the matrix form,

$$\mathbf{A}\cdot\mathbf{C}=\gamma\mathbf{C} \tag{20}$$

with the elements of the matrix $\mathbf{A}$ given by,

$$A_{mn}=(1/T_{m-1})\,U_{m-n}\,,\quad A_{mm}=(S_{m-1}/T_{m-1})\,. \tag{21}$$

Equation (20) is in the form of the characteristic equation of a matrix $\mathbf{A}$ which is asymmetric except in the case of zero tilt (i.e., $\alpha=0$). Hence, in general the eigenvalues and eigenvectors of (21) are complex. The eigenvectors are of course, the wave amplitudes of the various plane waves and the eigenvalues determine the wave points of Bloch waves on the dispersion surface. Note that a complex eigenvalue implies that the normal $\boldsymbol{n}'$ does not intersect the branches of dispersion surface. As may be seen in Fig. 2, this is only possible for very high angles of incidence (near grazing angle), where total reflection takes place. In the cases in which we are concerned, all the roots are purely real.

Given the various parameters of the crystal (lattice parameters, Fourier coefficients of potential), operating conditions of the microscope (e.g. accelerating voltage, magnification) and the conditions of tilt, we can calculate the matrix $\mathbf{A}$ from Equations (21). We are then able to calculate the wave vectors and amplitude coefficients of the Bloch waves excited in the crystal from Equation (20). The only other parameters necessary in order to have a complete knowledge of the wave function in the crystal are the excitation amplitudes of the Bloch waves $\psi^{(j)}$. These may be obtained by the application of the boundary conditions at the entrance surface of the crystal. The continuity of $\psi(\boldsymbol{r})$ and grad $\psi(\boldsymbol{r})$ at the entrance point should be a good approximation for all the angles of tilt used in the present calculations. In this case one may readily show that $\psi^{(j)}$'s are obtained by inverting matrix $\mathbf{C}$ and using the first column of $\mathbf{C}^{-1}$.

For the case of an untilted crystal, the above equations simplify considerably. Thus, substituting $\alpha=0$ in Eq. (21), we obtain,

$$A_{mn}=\frac{1}{2\sqrt{K^2-\chi^2\sin^2\beta}}\,U_{m-n}\,,$$
$$A_{mm}=\frac{g[2\chi\sin\beta\cos(\sigma-\omega)-g]}{2\sqrt{K^2-\chi^2\sin^2\beta}}\,. \tag{22}$$

The factor $\sqrt{K^2-\chi^2\sin^2\beta}$ in the denominator of Eq. (21) is in fact equal to K_z, the normal component of the refracted wave vector.

4. Backscattered Intensity

We employ the equations of Hirsch and Humphreys [1] to calculate the backscattered intensity. The theory is based on the assumption that local backscattering depends on the independent Bloch wave intensities rather than on the total wave intensity $\psi(\boldsymbol{r})\,\psi^*(\boldsymbol{r})$. Considering the scattering by a slab dz in a crystal of thickness t and assuming that there is conservation of electrons in the slice, Hirsch and Humphreys [1] derive the following equation for the backscattered intensity I_B,

$$I_B=\frac{1}{1+p^{(0)}t}\left\{p^{(0)}t+\sum_j I^{(j)}(0)\,\frac{p^{(j)}-p^{(0)}}{\mu^{(j)}}\cdot[1-\exp\{-\mu^{(j)}t\}]\right\}. \tag{23}$$

For the jth Bloch wave, $p^{(j)}$ (§ 5) and $\mu^{(j)}$ are the backscattering and absorption coefficients respectively and $I^{(j)}(0)$ is the intensity at the crystal surface. $p^{(0)}$ is the mean backscattering coefficient in the crystal. The absorption coefficients $\mu^{(j)}$ are related to the parameter $q^{(j)}$ discussed in § 2 by the simple relationship,

$$\mu^{(j)}=4\pi q^{(j)}\,. \tag{24}$$

It must be noted that because the energy losses have not been taken into account in the derivation of the above equation, it does not hold for thick crystals. In fact, it is necessary to introduce a "cut-off" thickness, t_b (Spencer et al. [9]). For $t<t_b$, the actual value of t is used in Equation (23). In bulk crystals, where $t>t_b$, t_b is substituted for t in the latter equation. The cut-off thickness t_b is related to the Bethe range R_B for the material and the electron energy considered (Spencer et al. [9]).

5. Backscattering Coefficients

We shall follow the method of Hirsch and Humphreys [1] in obtaining an analytical expression for the backscattering coefficients $p^{(j)}$. It is assumed that the main mechanism responsible for backscattering is phonon scattering. The two-beam equations of Hall and Hirsch [10] for thermal diffuse scattering are then generalized to the many-beam case. One obtains for the diffuse scattered intensity, $I_{TD}^{(j)}(s)$ due to the jth Bloch wave the following expression,

$$I_{\mathrm{TD}}(s) = \frac{N}{N_c}\,\psi^{*(j)}\,\psi^{(j)} \sum_g \sum_G C_g^{*(j)}\,C_G^{(j)} f_{s-g}\,f_{s-G} \cdot \{\exp(-M_{G-g}) - \exp[-(M_{s-g}+M_{s-G})]\} \sum_n^{N_c} \exp[2\pi i(\boldsymbol{G}-\boldsymbol{g})\cdot\boldsymbol{r}_n]\,. \quad (25)$$

N and N_c are the number of atoms in the crystal and the unit cell respectively. s is a deviation parameter corresponding to the angle through which the electron is scattered. f is the atomic scattering amplitude and $\exp(-M)$ is the Debye-Waller factor. The summation term in Eq. (25) represents a structure factor term. In Fig. 3, an incident beam of

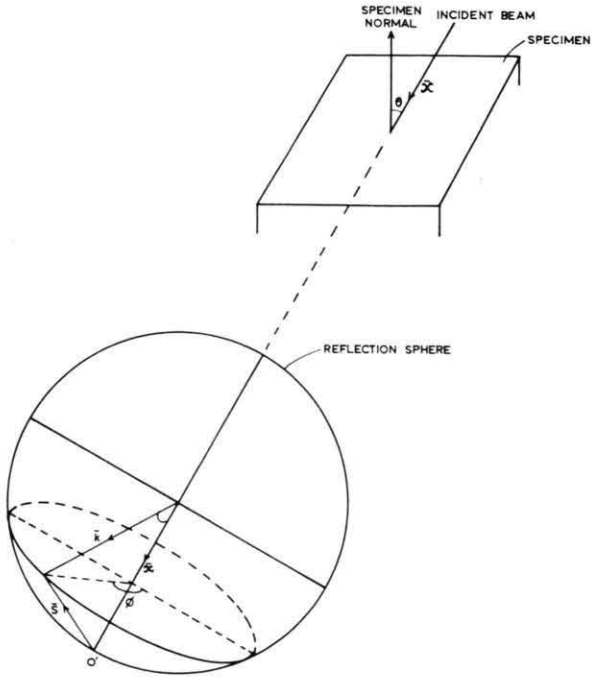

Fig. 3 The scattering of the incident beam through a vector $\boldsymbol{S}$. Coordinate Φ is also defined in the figure.

electrons is shown making an angle θ with the surface normal of the crystal. To obtain the backscattering coefficients, we need to find the fraction of electrons which are scattered into directions towards the surface. This implies that $I_{\mathrm{TD}}^{(j)}(s)$ as given by Eq. (25) should be integrated over the upper half of the reflection sphere,

$$p^{(j)} = \frac{\lambda^2}{N\,\Omega\,\psi^{*(j)}\,\psi^{(j)}} \iint_{s\,\Phi} I_{\mathrm{TD}}^{(j)}(s)\,s\,\mathrm{d}s\,\mathrm{d}\Phi\,. \quad (26)$$

Now, except at very high angles of tilt ($\theta > 75^\circ$), s is sufficiently large that Rutherford backscattering may be safely used to obtain the scattering amplitudes, i. e.,

$$f_{s-g} \cong f_{s-G} \cong f_s \cong \frac{2\,m\,e^2\,Z}{h^2}\,\frac{1}{s^2}\,. \quad (27)$$

Also, since M_s is proportional to s^2, the Debye-Waller factors are negligible, i. e.,

$$\exp(-M_{s-g}) \cong \exp(-M_{s-G}) \cong \exp(-M_s) \cong 0\,.$$

Using these relations in Eq. (26), we obtain,

$$p^{(j)} = \frac{\lambda^2}{N_c} \sum_n^{N_c} \exp[2\pi i(\boldsymbol{G}-\boldsymbol{g})\cdot\boldsymbol{r}] \cdot \{\sum_g \sum_G C_g^{*(j)}\,C_G^{(j)} \exp(-M_{G-g}) \iint_{s\,\Phi} \mathrm{d}s\,\mathrm{d}\Phi\}.$$

To carry out the double integration over the upper half of the reflection sphere, a new set of coordinates s' and Φ' are defined (see Figure 4). The origin 0

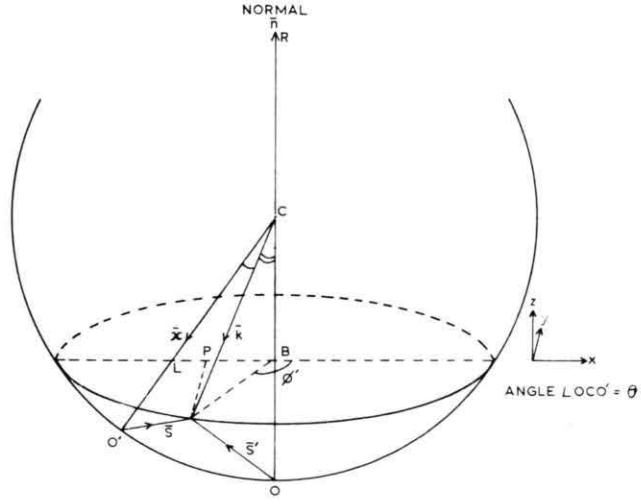

Fig. 4. The definition of the new coordinates s' and Φ' with respect to the old coordinates s and Φ.

is taken at the intersection of the surface normal with the reflection sphere (Figure 4). By transforming the old coordinates s und Φ to the new coordinates s' and Φ', we finally obtain the following expression for $p^{(j)}$,

$$p^{(j)} = \frac{F}{N_c\,\Omega}\left(\frac{2\,m\,e^2\,Z\,\lambda^2}{h^2}\right)^2 \sum_g \sum_G C_g^{*(j)}\,C_G^{(j)} \cdot \exp(-M_{G-g}) \sum_n^{N_c} \exp[2\pi i(\boldsymbol{G}-\boldsymbol{g})\cdot\boldsymbol{r}_n] \quad (28)$$

where F is the following double integral,

$$F = \int_{\eta=\sqrt{2}}^{\eta=2} \int_{\Phi'=0}^{\Phi'=2\pi} \frac{\eta\,\mathrm{d}\eta\,\mathrm{d}\Phi'}{[2(1-\cos\theta) + \eta^2\cos\theta + \eta\sqrt{4-\eta^2}\cos\Phi'\sin\theta]^2}\,. \quad (29)$$

F is basically a topographical factor arising because of the specimen tilt. The double integral in Eq. (29) has been numerically evaluated and is shown plotted against θ in Figure 5. At $\theta = 0$, i. e. when the

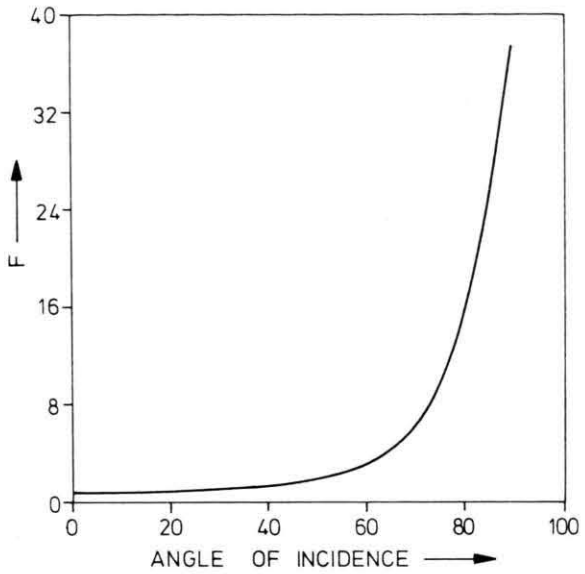

Fig. 5. The variation of the topographical factor F as a function of the angle of incidence θ.

beam is normal to the crystal surface, $F = \pi/4$ and Eq. (29) reduces to the expression given by Hirsch and Humphreys [1].

6. Calculation and Results

The parameters U_g, related to the Fourier coefficients of potential were evaluated using the scattering amplitudes of Doyle and Turner [11] and corrected for the Debye-Waller factor.

The parameters U_g', related to the Fourier coefficients of the imaginary potential [see Eq. (7)] were calculated in the same manner as Humphreys and Hirsch [12], but again using the more recent scattering amplitudes of Doyle and Turner [11]. Use of such scattering amplitudes resulted in slightly higher values for the absorption parameters U_g'/U_g as compared to those given by Humphreys and Hirsch [12].

To simplify the remainder of the calculations, the topographical factor F was assumed constant at the value of θ for the undeflected beam during the whole scan, i. e. it was assumed that $\theta = \alpha$ for all the points on the observation screen.

The equations presented in § 3 permit the computation of backscattered intensity for beam orientations corresponding to each point (x, y) on the observation screen. An example of this is the two-dimensional pattern for the (111) surface of an untilted silicon crystal shown in Figure 6 a. The reflections considered in the computations are shown in Figure 6 b. An accelerating voltage of 20 kv was assumed and the crystal thickness was set to 2 μm. Ten levels of greyness were used in the construction of this figure. Clearly better pictures may be obtained by increasing the number of reflections in the calculations and the number of grey levels in the construction.

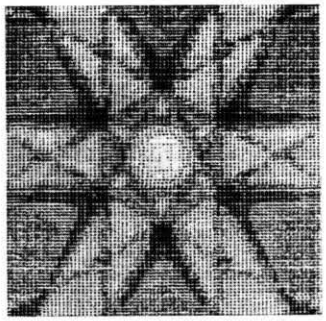

Fig. 6 a

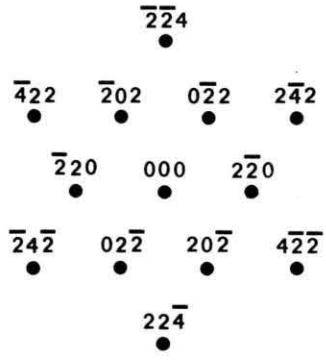

Fig. 6 b

Fig. 6. a) Computer simulated pattern for the (111) surface of an untilted crystal of silicon. b) The reflections used in the computation of Figure 6 a.

Some intensity profiles for tilted and untilted crystals are shown in Figure 7. The computations pertain to the 220 row of reflections in silicon with the crystal thickness set as 2 μm and accelerating voltage of the microscope set to 20 kV. Thirteen beams were used in all these calculations. A few points should be noted in these figures. In Fig. 7 a, the untilted case is shown where the central band

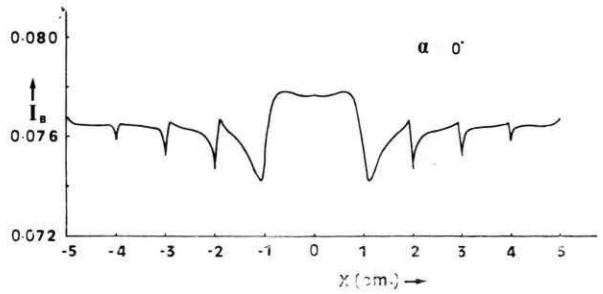

Fig. 7 a

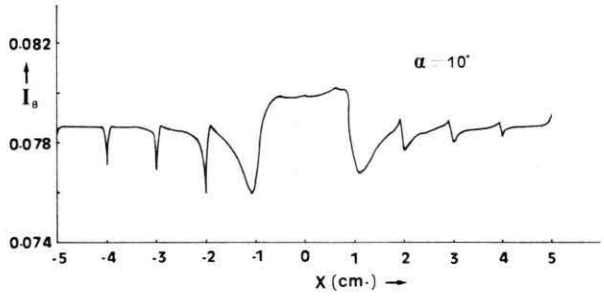

Fig. 7 b

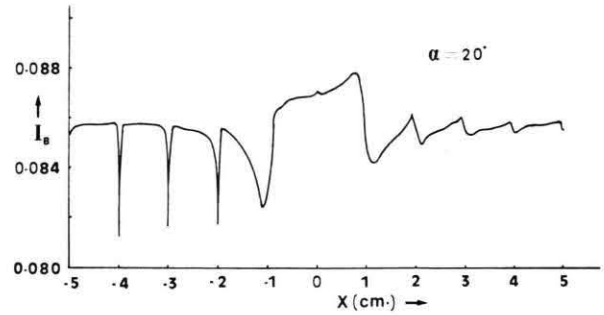

Fig. 7 c

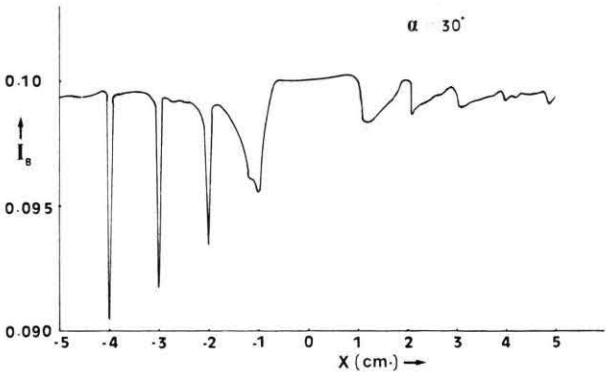

Fig. 7 d

Fig. 7. Intensity profiles for the 220 row of reflections in a crystal of silicon for various angles of tilt. The position of the $n\,\boldsymbol{g}$ Bragg reflection corresponds very closely to n cm. in these and the following figures.

and channeling lines are all symmetrical about the centre. Considerable contrast is obtained up to the third order reflection corresponding to the 660 Bragg position. The variation in contrast across the higher order lines is too small to produce any noticeable peak or dip in the backscattered intensity.

Figures 7 b to 7 d correspond to the same set of reflections but with the specimen surface inclined at 10°, 20° and 30° respectively with the 220 reciprocal lattice vector. The asymmetry is clearly shown with the edges on the "uphill" side becoming more pronounced as the angle of tilt increases. Use of the correct topographical factor for each individual point (see above) would slant each whole profile (except for $\alpha = 0$) slightly down on the left and up on the right. The effect of asymmetry is particularly noticeable on the lines rather than the central band. It may be noted that the maximum dip on the "downhill" side moves from the $\bar{2}\bar{2}0$ to $\bar{4}\bar{4}0$ to $\bar{6}\bar{6}0$ reflections as the angle of tilt increases from 0° to 10° to 20° respectively. It is also interesting to note that higher order reflections are now excited. Anomalies in contrast at the 880 and 10 10 0 Bragg positions are becoming important as the tilt increases.

Finally, Figs. 8 a and 8 b compare the simulated patterns for an untilted and a tilted crystal ($\alpha = 30°$) of silicon respectively. In this case the non-systematic reflections have been ignored (in contrast to Fig. 6) and only the 220 row of reflections

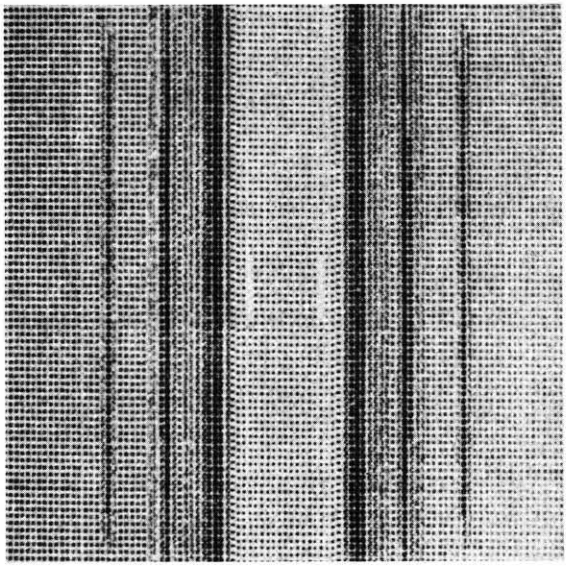

Fig. 8 a

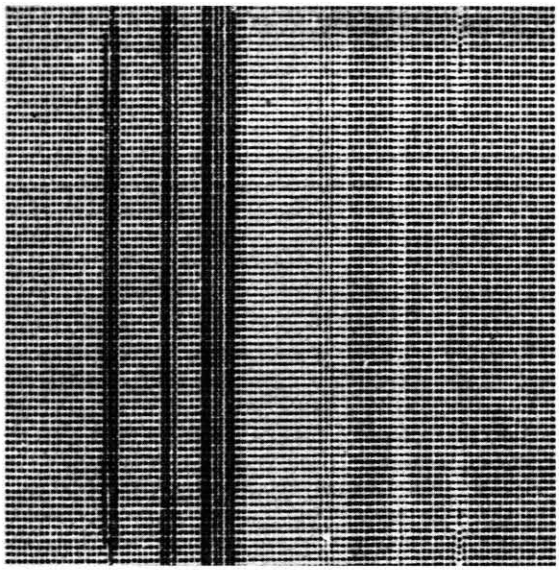

Fig. 8 b

Fig. 8. Computer simulated pattern for the 220 row of reflections in a silicon crystal, a) untilted; b) tilted through an angle of 30°.

has been considered. Although the neglect of non-systematic reflections is not very satisfactory in two-dimensional computations, the simulated patterns do indicate the effect of tilt on pseudo-Kikuchi bands and lines.

7. Discussion

In general, the $\mu^{(j)}$ terms in Eq. (23) determine the absorption of electrons belonging to the jth branch of the dispersion surface. The variation of backscattered intensity with beam orientation can, in fact be discussed in terms of the parameters $\psi^{(j)}$ which determine the excitation of the jth Bloch wave and the parameters $p^{(j)}$ which determines its rate of backscattering. We may therefore use the following approximate expression for the relative backscattered intensity,

$$\Delta I_B = \sum_j |\psi^j|^2 (p^{(j)} - p^{(0)}). \qquad (30)$$

The variations of $\psi^{(j)}$ and $p^{(j)}$ with beam orientation are shown in Fig. 9 for the 220 row of reflections in an untilted crystal of silicon. For clarity, only the values for the first four waves are shown in the figures. Hirsch and Humphreys [1], in fact have already discussed the variations of backscattered intensity for the untilted case, in terms of such

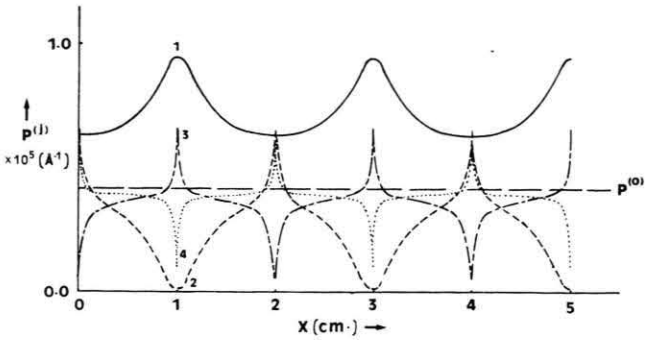

Fig. 9 a

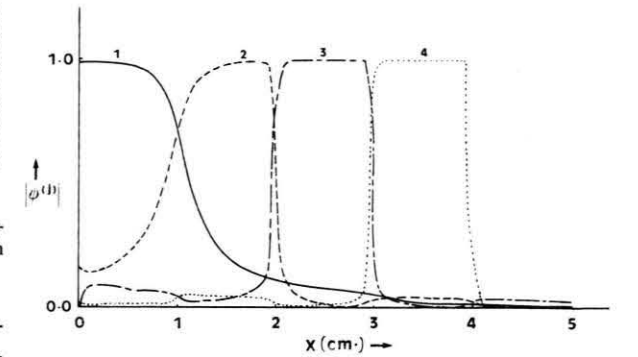

Fig. 9 b

Fig. 9. a) Variations of the backscattering coefficient $p^{(j)}$ with the beam orientation. b) Excitation coefficients of Bloch waves $\psi^{(j)}$ as a function of beam orientation. Only the first four waves are shown for clarity.

diagrams. However, we shall use such profiles to explain the asymmetry produced in the case of tilted crystals.

In the vicinity of a Bragg reflection, $n\boldsymbol{g}$, there are essentially two Bloch waves corresponding to $j = n$ and $j = n+1$ which are strongly excited in the crystal [13]. This is especially, true in scanning electron microscopy, where voltages of the order of $20 - 30$ kV are used and hence the excitation of other Bloch waves are not too strong. Now from Fig. 9 a, it will be noticed that at the $n\boldsymbol{g}$ Bragg position, $p^{(n)}$ always has a peak and $p^{(n+1)}$ has a dip. It is clear then that near such a reflection $(p^{(n)} - p^{(0)})$ is a positive quantity whereas $(p^{(n+1)} - p^{(0)})$ is a negative quantity. We can therefore rewrite (30) approximately as follows,

$$\Delta I_B \cong |\psi^{(n)}|^2 |p^{(n)} - p^{(0)}| - |\psi^{(n+1)}| |p^{(n+1)} - p^{(0)}|. \qquad (31)$$

From Fig. 9, we can see that just to the negative of $n\boldsymbol{g}$ reflection, a high value of $\psi^{(n)}$ coincides with

a high value of $p^{(n)}$ which from Eq. (31) corresponds to a high backscattered intensity. As we go through the Bragg position, $\psi^{(n)}$ decreases while $\psi^{(n+1)}$ correspondingly increases. Since $(n+1)$th wave has a low backscattering coefficient around this reflection, the backscattered intensity as a whole decreases. The overall form of the intensity profile around the $n\boldsymbol{g}$ reflection is therefore a maximum just negative of the reflection which passes into a minimum as shown in Figure 7 a.

Evidently the same situation holds for the other half of the profile because both $\psi^{(j)}$ and $p^{(j)}$ curves are symmetrical about the central position. In the case of an untilted crystal, we therefore have a symmetrical intensity profile around the central position.

When the crystal is tilted, the Bloch wave fields in the crystal are affected. With a tilt in the positive sense (as in Fig. 1), there is a movement in the profile of the excitation coefficients $\psi^{(j)}$ slightly to the left and parallel to the abscissa axis. These movements are particularly noticeable in the vicinity of Bragg positions and occur in the same direction on both sides of the central position. In Table 1, the values of $\psi^{(3)}$ and $\psi^{(4)}$ are compared around the 660 and $\bar{6}\bar{6}0$ reflections for a tilted and an untilted crystal.

Table 1

x (cm)	$\lvert\psi^{(3)}\rvert$ $\alpha=0°$	$\alpha=30°$	$\lvert\psi^{(4)}\rvert$ $\alpha=0°$	$\alpha=30°$	
−2.9	0.996	0.996	0.057	0.052	
−3.0	0.344	0.612	0.937	0.743	$x_{\bar{6}\bar{6}0}=-2.98$ cm
−3.1	0.044	0.048	0.997	0.996	
+2.9	0.996	0.996	0.057	0.063	
+3.0	0.344	0.225	0.937	0.980	$x_{660}=+2.98$ cm
+3.1	0.044	0.040	0.997	0.998	

These movements have a considerable effect on the backscattered intensity as may be explained by reference to the $\psi^{(j)}$ and $p^{(j)}$ profiles. As an example consider the situation around the 660 Bragg reflection in which case the strongly excited Bloch waves are 3 and 4 (Figure 10). When the crystal is tilted, the two waves move slightly to the left and therefore the position at which they have equal excitations no longer coincides with the dip and peak in $p^{(j)}$ (Figure 10). There is a basic difference, however, between the effect of tilt on the $\bar{6}\bar{6}0$ reflection and the effect on the 660 reflection.

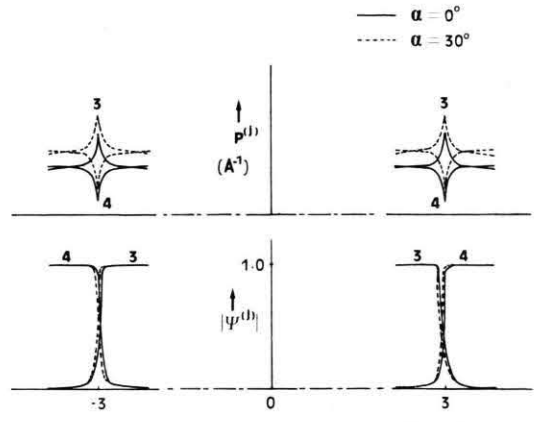

Fig. 10. Sketch of the variation of (a) $p^{(3)}$, $p^{(4)}$ and (b) $\psi^{(3)}$, $\psi^{(4)}$ with beam orientation and specimen tilt in the vicinity of the 660 and $\bar{6}\bar{6}0$ Bragg position.

Around the 660 reflection, as may be seen from Fig. 10, the peak of $p^{(3)}$ coincides with a lower value of $\psi^{(3)}$, whereas the dip in $p^{(4)}$ coincides with a higher value of $\psi^{(4)}$ as compared to the untilted case. In terms of Eq. (31), this corresponds to a relative decrease in the first term and a relative increase in the second term of the R.H.S. The net effect is a reduction in the relative backscattered intensity.

Around the $\bar{6}\bar{6}0$ reflection, a reverse effect takes place. The peak of $p^{(3)}$ coincides with a higher value of $\psi^{(3)}$, whereas the dip in $p^{(4)}$ coincides with a lower value of $\psi^{(4)}$. Therefore, there is a relative increase in the first term and a relative decrease in the second term of the R.H.S. of Equation (31). The net effect is hence an increase in the relative backscattered intensity on this side of the profile.

It is therefore possible to explain the asymmetry in the intensity profile for a tilted crystal in terms of the asymmetry in the excitation coefficients of Bloch waves. This model also shows that the effect of tilt is more pronounced on higher order channeling lines as compared to the central band. For the first order reflection, the important Bloch waves are (1) and (2) neither of which have a sharp peak or dip at the 220 Bragg position. Therefore the effect of tilt on the edges of the central band is not as pronounced as the effect on the second or third order channeling lines. In fact, since the peaks and dips are so sharp for higher numbered waves, a very slight movement is sufficient to make the peak or dip in $p^{(j)}$ coincide with the flat high/low parts of $\psi^{(j)}$ or $\psi^{(j+1)}$ profiles.

Another point to make is that the movement of $\gamma'^{(j)}$ profiles parallel to the abscissa axis are not equal for various Bloch waves. There is also a relative movement of the profiles with respect to one another which is enhanced as the angle of tilt is increased. The result is that the various Bragg reflections are differently affected as the angle of tilt increases (see Figure 7).

8. Conclusion

The contrast of pseudo-Kikuchi patterns from a tilted crystal is considered in terms of the Hirsch and Humphreys theory [1]. The effect of tilt on backscattering coefficients is taken into account and computations are made for various angles of tilt. The calculated intensity profiles show an asymmetry in the contrast of the opposite edges of a band in agreement with experimental results. This asymmetry is discussed in terms of the effect of tilt on the wavefields of incident electrons in the crystal. Some simulated patterns both for a tilted and for an untilted crystal are presented.

Acknowledgement

I would like to thank Dr. I. M. Boswarva for helpful advice and criticism in every stage of the work. The assistance of the staff of the Computer Advisory Service in Imperial College is also gratefully acknowledged.

[1] P. B. Hirsch and C. J. Humphreys, Proceedings Third Annual SEM Symposium, Chicago 1970, p. 449.
[2] E. Vicario, M. Pitaval, and G. Fontaine, C. R. Acad. Sci. Paris **270 B**, 1402 [1970].
[3] L. Reimer, H. G. Badde, H. Seidel, and W. Bühring, Z. Angew. Phys. **31**, 145 [1971].
[4] D. R. Clarke and A. Howie, Phil. Mag. **24**, 959 [1971].
[5] G. R. Booker in "Modern Diffraction and Imaging Techniques in Materials Science", edited by S. Amelinckx et al., North-Holland Publishing Co., Amsterdam 1970.
[6] J. P. Spencer and C. J. Humphreys, Electron Microscopy and Analysis, The Institute of Physics, Cambridge 1971.
[7] P. B. Hirsch, A. Howie, R. B. Nicholson, D. W. Pashley, and M. J. Whelan, Electron Microscopy of Thin Crystals, Butterworths, London 1965.
[8] In transmission electron microscopy the term "absorption" is commonly used for the cases where the inelastic processes scatter the fast electrons outside the objective apperture. This is due to the fact that in such cases the electrons do not reach the screen and are thus "effectively" absorbed.
[9] J. P. Spencer, C. J. Humphreys, and P. B. Hirsch, Phil. Mag. **26**, 193 [1972].
[10] C. R. Hall and P. B. Hirsch, Proc. Royal Soc. London **A 286**, 158 [1965].
[11] P. A. Doyle and P. S. Turner, Acta Crys. **A 24**, 390 [1968].
[12] C. J. Humphreys and P. B. Hirsch, Phil. Mag. **18**, 115 [1968].
[13] A. J. F. Metherell and R. M. Fisher, Phys. Stat. Sol. **32**, 551 [1969].